Analyst

Interdisciplinary detection science

www.rsc.org/analyst

Volume 136 | Number 8 | 21 April 2011 | Pages 1525–1768

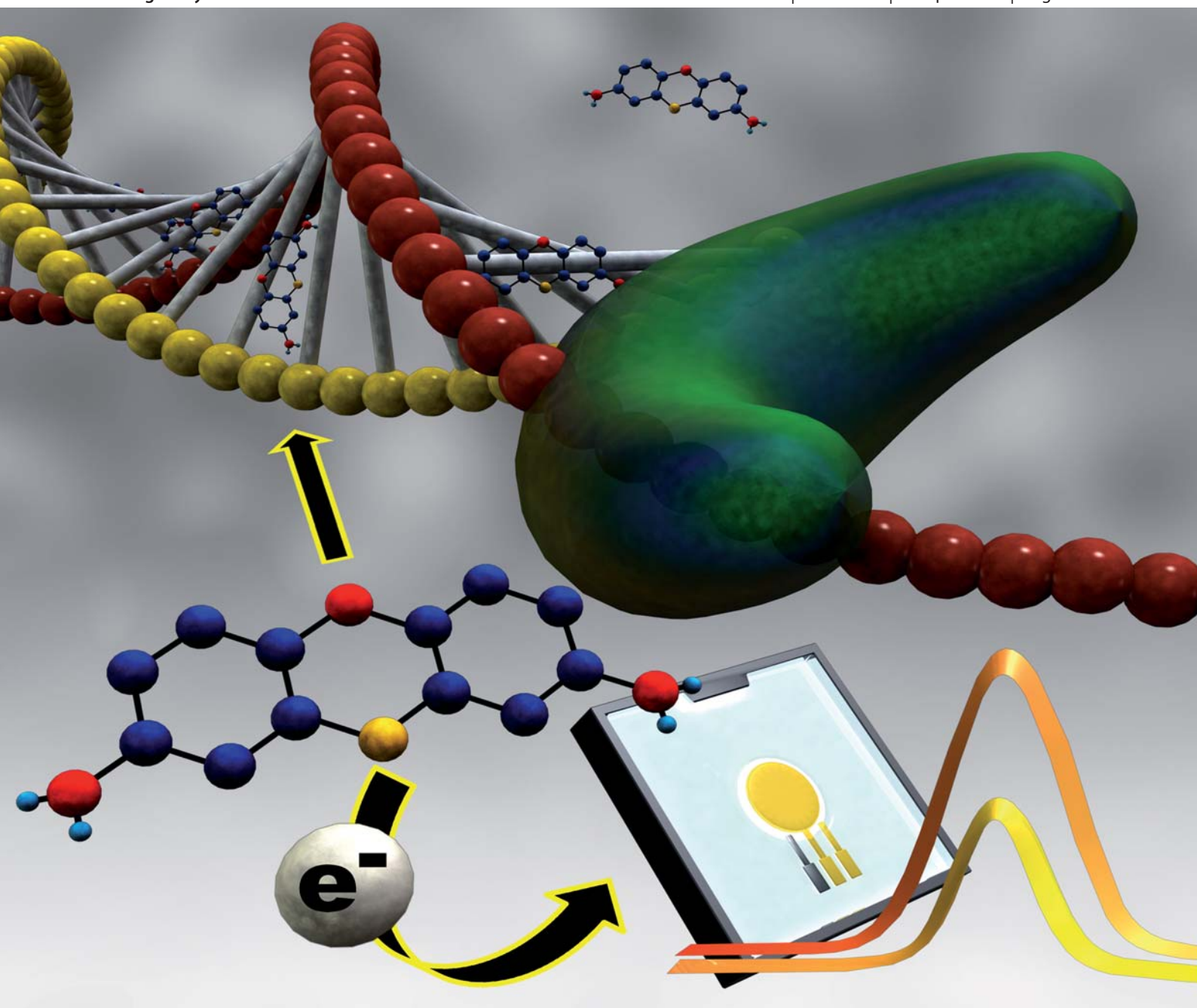

ISSN 0003-2654

RSC Publishing

PAPER

Hyun Gyu Park *et al.*

Investigation of the signaling mechanism and verification of the performance of an electrochemical real-time PCR system based on the interaction of methylene blue with DNA

0003-2654(2011)136:8;1-F

Analyst

Dynamic Article Links

Cite this: *Analyst*, 2011, **136**, 1573

www.rsc.org/analyst

PAPER

Investigation of the signaling mechanism and verification of the performance of an electrochemical real-time PCR system based on the interaction of methylene blue with DNA†

Byoung Yeon Won,[a] Sujeong Shin,[a] Songyi Baek,[a] Ye Lim Jung,[a] Taihua Li,[a] Sung Chul Shin,[a] Dae-Yeon Cho,[b] Sang Bok Lee[cd] and Hyun Gyu Park*[a]

Received 7th September 2010, Accepted 21st January 2011
DOI: 10.1039/c0an00695e

The operation of an electrochemical real-time PCR system, based on intercalative binding of methylene blue (MB) with dsDNA, has been demonstrated. PCR was performed on a fabricated electrode-patterned glass chip containing MB while recording the cathodic current peak by measuring the square wave voltammogram (SWV). The current peak signal was found to decrease with an increase in the PCR cycle number. This phenomenon was found to be mainly a consequence of the lower apparent diffusion rate of the MB-DNA complex ($D_b = 6.82 \times 10^{-6}$ cm^2 s^{-1} with 612 bp dsDNA) as compared to that of free MB ($D_f = 5.06 \times 10^{-5}$ cm^2 s^{-1}). Utilizing this signal changing mechanism, we successfully demonstrated the feasibility of an electrochemical real-time PCR system by accurately quantifying initial copy numbers of *Chlamydia trachomatis* DNA templates on a direct electrode chip. A standard calibration plot of the threshold cycle (C_t) value *versus* the log of the input template quantity demonstrated reliable linearity and a good PCR efficiency (106%) that is comparable to that of a conventional TaqMan probe-based real time PCR. Finally, the system developed in this effort can be employed as a key technology for the achievement of point-of-care genetic diagnosis based on the electrochemical real-time PCR.

1 Introduction

The real-time PCR technique has been used as a powerful method for the detection and quantitative analysis of nucleic acids in SNP genotyping, gene expression profiling, and genetic diagnosis. The clinical usage of this technique in the diagnosis of tumors and infectious diseases is becoming increasingly important.[1,2] The key feature of the real-time PCR is the quantification of target DNA during the PCR amplification process. In this way, the need for labor-intensive and time-consuming post-PCR analysis (*e.g.*, gel-based electrophoresis) can be eliminated. In addition, a unique feature of performing real-time PCR is found in the capability to accurately quantify initial target DNA with great specificity.[3] However, the currently developed methods not only require specialized reagents (fluorescent probes or DNA-binding dye) but also the instruments employed for monitoring fluorescence are bulky and relatively expensive. These limitations prevent widespread applications in facility-limited environments. With respect to the goal broadening its utility and overcoming these limitations, real-time PCR procedures that rely on electrochemical devices have become attractive detection platforms owing to their simplicity, portability and cost-effectiveness.[4–7]

Electrochemical real-time PCR can be accomplished utilizing the electrochemical characteristics of specially modified dNTP or free dNTP. Hsing and his coworkers recently described a solid-phase electrochemical real-time PCR system that operates in a silicon–glass microchip.[8,9] This method, employing ferrocene-tagged dUTP, was used to monitor the current signal increase associated with base extension from primers immobilized on the electrode surface. Similarly, Marchal and his coworkers were able to monitor the consumption of DNA monomers during PCR by measuring the catalytic oxidation current[10–14] of free dGTP or 7-deaza-dGTP in the presence of $Ru(bpy)_3^{3+}$ or $Os(bpy)_3^{3+}$ respectively.[15]

An alternative method, utilizing DNA-intercalative electroactive molecules, can be employed to detect amplified DNA based on differences between their electrochemical reaction rates before and after binding with DNA. An example of the validity of this approach came from studies by Bard and his coworkers,[16,17] which demonstrated that an electrochemical

[a]*Department of Chemical and Biomolecular Engineering, KAIST, Daejeon, 305-701, Republic of Korea. E-mail: hgpark@kaist.ac.kr; Fax: +82 42 350 3910; Tel: +82 42 350 3932*
[b]*Clinical Research Institute, Labgenomics, Seoul, 137-874, Republic of Korea*
[c]*Department of Chemistry and Biochemistry, University of Maryland, College Park, MD, 20742, USA*
[d]*Graduate School of Nanoscience and Technology (WCU), KAIST, Daejeon, 305-701, Republic of Korea*
† Electronic supplementary information (ESI) available: Further experimental details and Fig. S1. See DOI: 10.1039/c0an00695e

current change occurs in a system comprised of a metallic intercalator in the presence of dsDNA. Also, Tamiya and his coworkers utilized this type of signal changing system to detect DNA after PCR using the Hoechst 33258 DNA intercalator.[18] Currently, the most frequently studied electroactive DNA intercalator in the electrochemical DNA detection field is methylene blue (MB).[19–23] Several reports exist describing MB binding to DNA.[24–27] Recently, Hai-Qing and his coworkers showed that electrochemical monitoring of PCR is possible with MB in a microfluidic device.[28] This DNA intercalator-based method for the development of electrochemical real-time PCR could be superior to the other method described above, which shows poor DNA amplification efficiency presumably caused by steric hindrance during solid-phase DNA hybridization or polymerization,[15,29,30] and the need for voltages higher than 1.0 V (*vs.* Ag/AgCl) to promote oxidation of guanine bases.[31] Although the previous study showed that the MB-based method produces reliable signal change during the PCR process, its focus was primarily on the design of the microfluidic device rather than on investigation of signaling mechanism. These workers assumed that electroinactivity caused by binding of MB to the PCR amplicon was a result of a much lower diffusion coefficient of the MB-DNA complex compared to that of free MB.

We felt that a mechanism study of the electrochemical signaling process would provide an essential foundation for the development of the electrochemical real-time PCR based on MB. For this purpose, we have explored the mechanism for electrochemical signaling by MB during PCR amplification under the PCR buffer and high temperature (72 °C) conditions. Theoretical currents arising in this system, estimated based on the multicomponent diffusion model[17,32] using concentrations of free MB and the MB–DNA complex determined by fluorescence titration of MB with DNA, were compared with experimentally recorded values. Finally, we demonstrated the feasibility of the electrochemical real-time PCR system on a fabricated electrode-patterned glass chip using *Chlamydia trachomatis* DNA as a target gene. A comparison of the results with those obtained using a conventional TaqMan probe based real-time PCR demonstrate the analytical capability of the MB based assay system.

2 Experimental

2.1 Reagents

Methylene blue, mercaptohexanol and bovine serum albumin (BSA) were purchased from Sigma-Aldrich. FastStart Taq DNA polymerase and i-Pfu DNA polymerase together with the corresponding PCR buffer and dNTPs were obtained from Roche (Germany) and iNtRON (Korea), respectively. The oligonucleotide primers and TaqMan probe were synthesized, purified by using HPLC, and confirmed by using MALDI-TOF by Genotech (Daejeon, Korea). All other materials used were the highest quality available. Doubly distilled water with a specific resistance over 18 MΩ·cm was used.

2.2 Investigation of the MB-based electrochemical signaling mechanism

dsDNA (475 nM, 612 bp), obtained from secondary PCR (see SI), was resuspended in PCR buffer (pH 9.0) containing 30 mM Tris-HCl, 20 mM salts (Na^+ and NH_4^{2+}) and 2 mM Mg^{2+}. Two μL of the dsDNA solution was added to a 62.4 μM MB solution prepared in the same buffer at 72 °C. The fluorescence intensity of the solution was then measured at 684 nm with excitation at 668 nm light. Addition of the dsDNA solution was repeated until the decrease in the fluorescence signal ceased. The association constant for MB and dsDNA was calculated by using the Scatchard equation of $r/c = nK_a - rK_a$, where r = [bound MB]/[total binding sites in DNA], c = [free MB], n = number of binding site per DNA base pair, and K_a = association constant. For the successively diluted samples, background-subtracted cyclic voltammograms (CV) were also recorded using an electrochemical analyzer (Gamry, Reference 600, Warminster, PA) under 100 mV s^{-1} scan rate.

To determine the apparent diffusion coefficient of free MB (D_f) and the MB–DNA complex (D_b), MB–DNA complex was prepared by mixing 62.4 μM of MB and 4.1 μM of 612 bp dsDNA which corresponded to 2.5 mM of total base pairs ([DNA base pair]/[MB] = 40). The cathodic peaks of background-subtracted CVs were recorded by using 10–200 mV s^{-1} scan rates, and the CV under 100 mV s^{-1} was employed to investigate the change of the heterogeneous electron transfer rate of MB after binding with dsDNA.

2.3 Electrodes patterning on glass chip

A Pyrex glass wafer (1 mm thickness) was treated by using the standard wet-clean process by SPM (sulfuric acid peroxide mixture)/SC1 (standard clean-1, ammonium peroxide mixture) and coated with 20 nm of chrome followed by formation of a 20 nm gold layer by sputtering. The spin-coated wafer with DS-S700 positive photoresist (PR) was soft-baked in a 90 °C convection oven for 270 s and UV-irradiated (29 m·W·cm^{-2}) through the patterned mask. The wafer was then placed in DTD200 developer for 60 s and hard-baked for 10 min at 110 °C. The gold and chrome layer on the wafer were successively removed by using a KI and I_2 solution and standard chrome etchant, respectively. Finally, the PR was oxidized with piranha solution (3 : 1 mixture of concentrated H_2SO_4 and H_2O_2).

A pseudo-reference Ag/AgCl electrode was fabricated on the gold reference electrode patterned on a glass chip by silver and silver chloride deposition.[33,34] A cleaning step was performed with the potential cycling from 0 to 1.3 V with 0.3 V s^{-1} scan rate for 2 h in 10 mM H_2SO_4. Electro-deposition of the silver layer was then conducted in 2 mM $AgNO_3$ by applying reduction potential (0 to −0.4 V) under a 0.5 mV s^{-1} scan rate in the presence of a additional platinum counter electrode and Ag/AgCl reference electrode. The deposited silver layer was oxidized by cycling the potential back to 0.4 V in 1 mM NaCl and 0.4 V was applied until the oxidation current decreased to background. The final electrode-patterned glass chip was cleaned by sonication for 5 min and thoroughly washed with deionized water.

2.4 Monitoring of DNA amplification during PCR

The working electrode, patterned on the glass chip, was modified with 1 mM mercaptohexanol for 30 min. The adhesive frame seal incubation chamber (9 × 9 mm, 25 μL, Bio-rad)[35] was attached

to the electrode-patterned glass chip, and 25 μL of reaction mixture containing 0.1 mM dNTPs, 0–10^7 copy number of template, 0.25 μM of each primer (forward: 5′-CCATCTTCTTTGAAGCGTTGT and reverse: 5′-ACAG-GATGACTCAAGGAATAG), 3.3 U of i-Pfu Taq polymerase, 171 μg bovine serum albumin (BSA), 10 μM MB prepared in PCR buffer (30 mM Tris-HCl, 2 mM Mg^{2+}, and 20 mM salts consisting of Na^+ and NH_4^{2+}) was added to the chamber. The coverslip was carefully placed to prevent bubble formation in the chamber and the assembled PCR chip was introduced onto a slide griddle adaptor (SGP-0196, MJ research, Waltham, MA) with a droplet of mineral oil at the contact plane between the PCR chip and slide griddle adaptor. The adaptor was put on the PCT-0200 thermal cycler and PCR was performed (10 min at 95 °C, followed by 40 cycles of 60 s at 95 °C, 60 s at 55 °C, and 60 s at 72 °C) using the "Lid-heating OFF" mode. Simultaneously, square wave voltammetry (SWV) was performed following every extension step with a CH instrument 620B electrochemical analyzer (Austin, TX) coupled with desktop computer for data acquisition. The following parameters were employed for SWV: initial potential = 0.05 V, final potential = –0.35 V, potential increment = 0.002 V, amplitude = 0.05 V and frequency = 10 Hz.

3 Results and discussion

3.1 Investigation of signaling mechanism of MB-based electrochemical real-time PCR

A thorough consideration of all of the possible strategies for electrochemical real-time PCR monitoring (see Table 1) led us to conclude that a strategy based on the use of the DNA-binding molecule MB was most suitable. Fig. 1A contains a schematic illustration of the process in which the electrochemical signal associated with MB decreases as the concentration of DNA increases during PCR. Basically, the system is comprised of free and DNA-bound MB, both of which have the same redox potential. The intensities of the current signals from both species, however, will differ owing to the fact that rate of the electrochemical reaction of MB should decrease after binding with DNA. Thus, DNA amplification taking place in the PCR process can be monitored by measuring the extent of the decrease in the current of the PCR mixture. It is assumed that at the beginning of the PCR process, only free MB exists in the mixture. As the concentration of DNA increases with each PCR cycle number, the concentration of free MB decreases in concert with an increase in the concentration of the MB–DNA complex. The reaction rate of the system decreases with time leading to

Table 1 Summary of possible key strategies to obtain electrochemical signal during PCR

Target components	Electrochemical detection methods	Detection principles	Critical limitations
Generation of PPi[a]	Ion selective electrode (ISE)	PPi + H_2O → 2Pi[b] Dibasic phosphate-selective membrane[36]	Signal disturbance by other salts in the PCR buffer
	Cobalt electrode[37,38]	PPi + H_2O → 2Pi Selective response of a cobalt electrode towards dibasic phosphate	Insufficient detection limit (> 5 μM) to monitor the produced PPi during PCR
	Enzymatic electrocatalysis[39]	Pyrophosphatase: PPi → 2Pi PNP[c]: Pi + xanthosine → xanthine + α-D-ribose-1-phosphate XOD[d]: xanthine → uric acid + e^-	Too low electrocatalysis rate to observe the electrochemical signal (below 0.5 mV s^{-1} scan rate) under PCR condition
	Impedance spectroscopy	Capacitance variation of PCR buffer at the electrode surface caused by the increase of phosphate ion concentration	Signal disturbance by excess amount of other ions in PCR buffer
Generation of dsDNA	Direct oxidation[e]	Electrochemical oxidation of purine bases[40,41]	Signal disturbance byoxidation of free dGTP or dATP
	Modified dNTPs[8,9]	Modification of dNTPs with electrochemical signaling molecules	Signal disturbance by the free signaling molecule-modified dNTPs
	DNA-binding molecules	Electrostatic binding of ruthenium hexamine	Low signal resolution due to the weak binding affinity to dsDNA under PCR condition
		Intercalative binding of methylene blue[28]	Possible signal disturbance by MB–ssDNA binding through MB–guanine interaction[19,42]
Consumption of dNTPs	Impedance spectroscopy	Capacitance variation of PCR buffer at the electrode surface caused by the decrease of dNTP ion concentration	Low signal resolution due to the excess amount of free dNTPs compared to the amount of consumed dNTPs during PCR
	Oxidation of dNTPs	Direct oxidation of free dGTP or dATP[e] Electrocatalytic oxidation of free dGTP in the presence of electron mediators[15]	

[a] Pyrophosphate. [b] Phosphate. [c] Purine nucleoside phosphorylase. [d] Xanthine oxidase. [e] The direct oxidation method destroys DNA in the sample and this is a critical disadvantage.

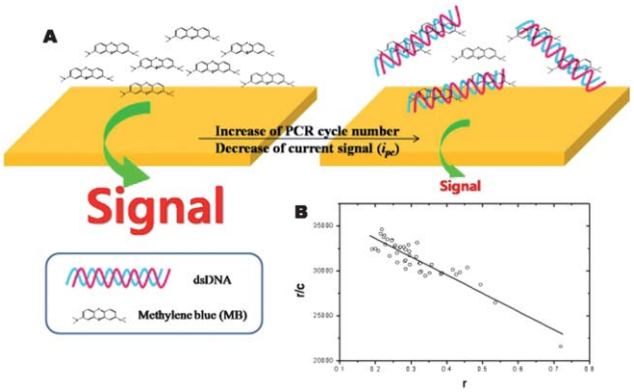

Fig. 1 Schematic illustration of the electrochemical signal decrease with increasing PCR cycle number (A) and Scatchard plot of data obtained from the spectrofluorometric titration of MB with dsDNA (B), where, r = [bound MB]/[total binding sites in DNA] and c = [free MB].

a decrease of the electrochemical signal paralleling the progress of PCR. In this system, the reaction rate can be determined by several factors including the diffusion rates of MB and the MB–DNA complex, the affinity of MB and the MB–DNA complex to the electrode surface, and the heterogeneous electron transfer rate between MB and the electrode.

To confirm the binding of MB to DNA under the PCR conditions, spectrofluorometric titration of MB with DNA was performed. As shown in Fig. 1B, a Scatchard plot derived from the titration data is linear and the slope of this plot gives this the association constant (K_a) for complex formation of 2.02×10^4 M^{-1}. The magnitude of K_a is consistent with those reported for MB–DNA interaction,[24,26,27] a result that indicates that MB is tightly bound to DNA even under the PCR salt composition and the high temperature (72 °C) conditions. The Y-intercept of the plot shows that the maximum number of bound MB per binding site (DNA base pair) is 1.8. This unexpected value that is higher than 1.0 indicates that another type of interaction (e.g. electrostatic) exists between MB and DNA in addition to intercalative binding.

Following confirmation of MB–DNA complex formation, CV measurements were performed on free MB and the MB–DNA complex in order to determine their individual electrochemical reaction rates. Typical CV spectra (v = 100 mV s^{-1}) of 62.4 μM MB in the absence and presence of DNA are shown in Fig. 2A. A decreased peak current with a positive shift of both anodic and cathodic peaks was observed in the presence of DNA, which is a typical characteristic associated with the intercalation of small molecules with DNA.[17,43] The CV of free MB (Fig. 2A, dashed line) shows that its reduction takes place with a cathodic peak potential of E_{pc} of –0.284 V *vs.* pseudo Ag/AgCl. Reoxidation occurs at –0.234 V (E_{pa}) upon scan reversal. The separation of the anodic and cathodic peak potentials (ΔE_p = 49.8 mV) indicates that a quasi-reversible two-electron redox reaction is occurring (0.069/n volts at 72 °C). In the presence of dsDNA (612 bp, 4.1 μM, and 2.5 mM of base pairs) at the same concentration as MB, E_{pc} and E_{pa} are –0.254 and –0.204 V, respectively. The value of ΔE_p in the presence of DNA is still 49.9 mV, showing that reversibility of the electron transfer process is maintained when DNA is present. Additionally, the

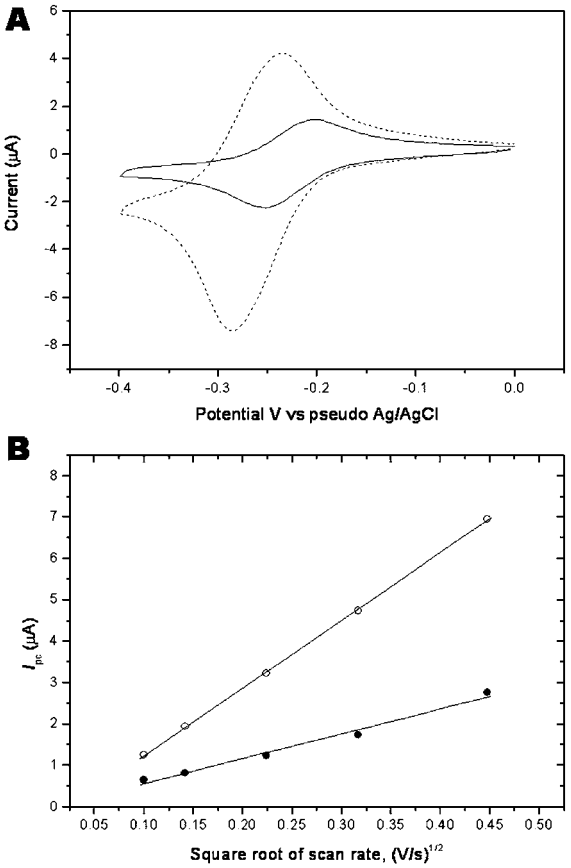

Fig. 2 (A) Cyclic voltammograms of MB with (solid line) and without (dashed line) DNA in PCR buffer (see text). [DNA base pair]/[MB] ratio was 40. 100 mV s^{-1} scan rate was applied. (B) Plots of cathodic peak currents *vs.* square roots of scan rates recorded with free MB (open circle) and MB–DNA complex (solid circle). The measurement conditions were same as with (A).

constancy of the ΔE_p values in the CVs of both free MB and the MB–DNA complex indicates that the heterogeneous electron transfer rates of both species are the same under the measurement condition. In Fig. 2B are displayed plots of cathodic peak currents, i_{pc} *vs.* the square roots of the scan rates ($v^{1/2}$). In the case of both free MB and the MB–DNA complex, the plots are linear indicating that the current signal is mainly controlled by diffusion and that there is no significant contribution by physical adsorption of MB or MB–DNA to the electrode surface. The fact that the slope of the i_{pc}–$v^{1/2}$ plot of MB–DNA complex is much lower than that of free MB indicates that a significant reduction occurs in the apparent diffusion coefficient when the MB–DNA complex forms. Based on the slopes of the plots, the apparent diffusion coefficients are estimated to be 5.06×10^{-5} cm^2 s^{-1} and 6.82×10^{-6} cm^2 s^{-1} for free MB (D_f) and DNA-bound MB (D_b), respectively. These observations lead to the conclusion that the decrease seen in the electrochemical reaction rate of MB with increasing DNA concentration is mainly a consequence of the decrease in the apparent diffusion coefficient of MB after the formation of MB-DNA complex.

For the purpose of confirming that the PCR monitoring system is governed mainly by diffusion, a multicomponent diffusion model[16,17,32] was employed to estimate the

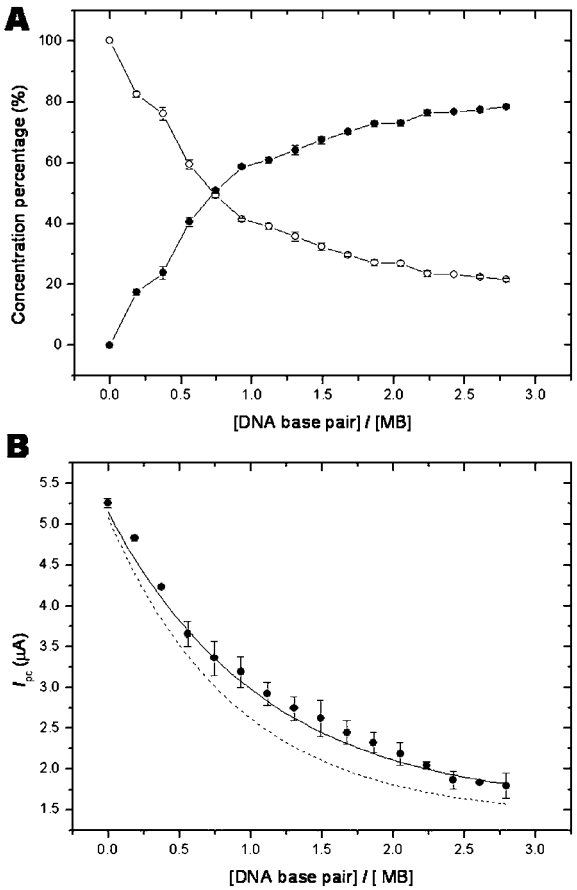

Fig. 3 The concentration percentage of free MB (open circle) and DNA-bound MB (solid circle) with increasing [DNA base pair]/[MB] determined by fluorescence titration. (B) Estimated cathodic peak currents of CV with static (dashed line) and mobile (solid line) models along with the experimental data (solid circle).

electrochemical current signal observed experimentally. Based on the decrease of fluorescence intensity with increasing DNA concentration depicted in Fig. 1B, the concentration of free MB (C_f) and the DNA–MB complex (C_b) with increasing [DNA base pair]/[MB] was calculated (Fig. 3A). The calculated values were employed to estimate the current peak signal *versus* the concentration ratio [DNA base pair]/[MB]. Under the experimental conditions, two limiting possibilities exist for the current signal seen in the CV spectra that depend on the mode of interconversion between free MB and bound MB. The interconversion can be treated as either being static[44] or mobile,[45–48] which correspond to no interconversion (eqn (1)) or rapid interconversion (eqn (2)) during a scan on the time scale of the CV experiment, respectively,

$$i_{pc} = B(D_f^{1/2}C_f + D_b^{1/2}C_b) \quad (1)$$

$$i_{pc} = BC_t(D_fX_f + D_bX_b)^{1/2} \quad (2)$$

where $B = 0.4463n^{3/2}F^{3/2}R^{-1/2}T^{-1/2}Av^{1/2} = 2.49 \times 10^5 n^{3/2}Av^{1/2}$ (at 72 °C), $X_f = C_f/C_t$, $X_b = C_b/C_t$, i_{pc} is total cathodic current, n is the number of electrons transferred per MB molecule, F is the Faraday constant, A is the electrode surface area, C_t is the total concentration of MB, v is the scan rate, D_f is the diffusion coefficient of free MB, D_b is the apparent diffusion coefficient of DNA–MB complex, R is the ideal gas constant, and T is the temperature. Fig. 3B contains plots of the estimated values from the static (dashed line) and mobile (solid line) models together with the experimental values obtained from the electrochemical titration experiment (solid circle). As can be seen by viewing the plots, the experimental values are better fitted to the mobile model than to the static model. As a result, we suggest that rapid interconversion between free and bound MB takes place on the time scale of the voltammetric measurements in this system.

3.2 Electrochemical real-time PCR on electrode-patterned chip

In order to probe the feasibility of the electrochemical real-time PCR monitoring employing the signaling mechanism, an electrode-patterned glass chip (Fig. 4A) was fabricated and assembled onto a thermal cycler (Fig. 4B). For construction of chip-based PCR, several potential issues needed to be evaluated. Firstly, since the polymerase protein is susceptible to adsorption onto the glass surface or coverslip, a high concentration of polymerase is required and BSA needs to be added to block the glass surface and diminish the extent of polymerase adsorption. Otherwise, polymerase adsorption would cause an undesired effect on the electrochemical signal. It is noteworthy that proteins are not adsorbed onto the working electrode surface in our system because the electrode surface is modified with mercaptohexanol. Secondly, the reaction chamber on the PCR chip has to be perfectly sealed with a coverslip to prevent formation of air bubbles or evaporation of the PCR solution during thermal cycling. Lastly, direct and perfect contact between the PCR chip and griddle adaptor is required to enable efficient heat transfer from the thermo-block to the PCR chip. For this purpose, a droplet of mineral oil is applied at the contact plane between the PCR chip and griddle adaptor. Also, a slightly longer reaction time is allowed for each PCR step to ensure that the desired thermal cycling occurs even in the presence of the griddle adaptor between the PCR chip and the thermo-block.

To verify the performance of this electrochemical real-time PCR monitoring system, PCR with the model target *Chlamydia*

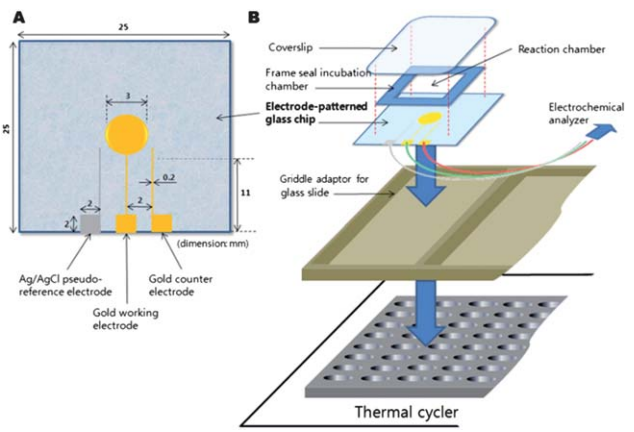

Fig. 4 Illustrations of the electrode-patterned glass chip (A) and installation of the chip onto thermal cycler (B) to achieve the electrochemical real-time PCR.

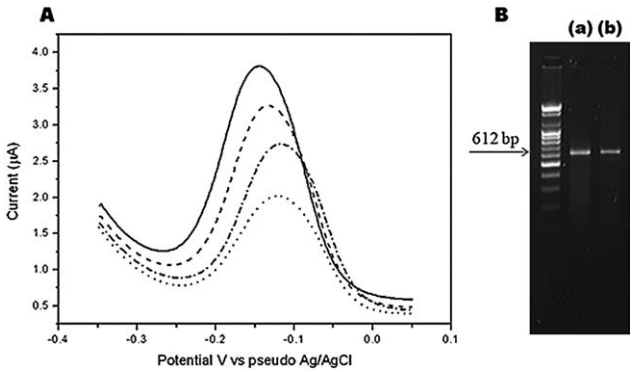

Fig. 5 (A) SWV pattern with increasing PCR cycle number: 0 cycle (solid line); 10 cycle (dashed line); 20 cycle (dash-dotted line); 40 cycle (dotted line). The potential was scanned from 0.05 V to –0.035 V with 0.002 V potential increment, 0.05 V amplitude and 10 Hz frequency. (B) Agarose gel electrophoresis image resulted from conventional tube-based PCR (a) and our chip-based PCR (b).

trachomatis gene was performed and SWV signals were recorded at the end of each extension step. SWV was employed instead of CV owing to its higher sensitivity and also since it provides peak-like shaped voltammograms. As the spectra in Fig. 5A show, a decrease in the SWV current signal takes place with increasing PCR cycle number. A slight peak shift to positive potential is observed as the PCR cycle number increases, a frequently observed phenomenon when a signaling molecule is bound to DNA.[17,43] However, this shift does not interfere with monitoring the process and, consequently, a reliable decrease in i_p is observed regardless of the E_p shift. Formation of the amplified PCR product was confirmed by using agarose gel electrophoresis. As shown in Fig. 5B, a clear band is obtained by utilizing the chip-based PCR method (b), which has nearly the same intensity as that produced by using a tube-based conventional PCR system (a). This result demonstrates that PCR takes place on the glass chip without inhibition caused by the presence of MB (10 μM).

In order to demonstrate the quantitative analysis capability of the electrochemical-based system, monitoring PCR using 0–10^7

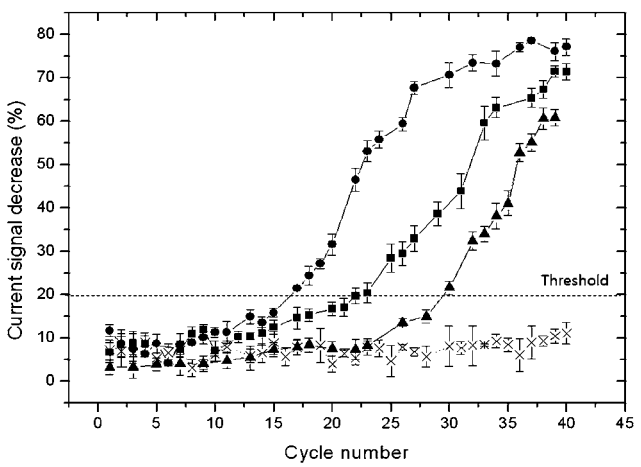

Fig. 6 Amplification curve obtained from the electrochemical real-time PCR system with serially diluted samples containing 10^7 (●), 10^5 (■), 10^3 (▲), and 0 (×) copy number of template. The horizontal dashed line indicates the threshold level used to establish the C_t values in Fig. 7.

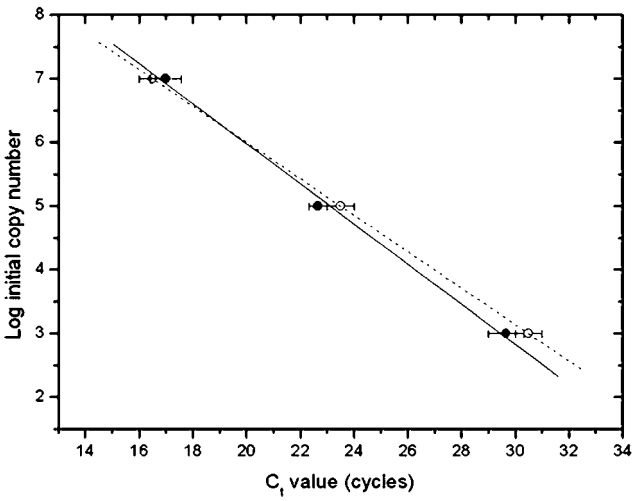

Fig. 7 Standard calibration plots of C_t *vs.* the logarithmic input of template copy number for conventional TaqMan probe-based real-time PCR (○) and our electrochemical real-time PCR (●). Both straight lines are linear regression.

initial copy numbers of templates were performed. In Fig. 6 is shown the results of electrochemical real-time monitoring of 5 equivalent experiments. The magnitude of the decrease in current signal with increasing cycle number is represented as a percentage of the current signal decrease relative to the initial value recorded before amplification. Throughout the process, reliable signal changes are obtained. Plots of the signals *versus* increasing PCR cycle number showed perfect exponential behavior. The signal from experiments without template did not change throughout the process indicating that non-specific DNA amplification or signaling did not take place. With the threshold value at 20% of *Y*-axis, the standard curve shown in Fig. 7 was obtained.

The C_t value of the real-time PCR method shows an excellent linear relationship with initial copy number of the template. This pattern compares favorably with the standard line generated by conventional TaqMan probe-based real-time PCR. Finally, the PCR efficiency was found to be 106%, which is within the generally acceptable range for the real-time PCR.[1,2]

4 Conclusions

In the investigation described above, we have designed, mechanistically explored and successfully tested an electrochemical real-time PCR system mounted on an electrode-patterned glass chip. Monitoring PCR by using this system is based on a decrease of apparent diffusion rate of MB after binding with amplified DNA. The system, exhibiting quantitative analytical capability over a range of initial DNA copy numbers, reliably produces changes in the current signal in a manner dependent on the increase in PCR cycle numbers. Moreover, the analysis produces results that are comparable to those coming from conventional TaqMan-based real-time PCR. The significant feature of this effort compared to those previously undertaken to explore the MB-based electrochemical real-time PCR method[28] is that it is the first in which a systematic study was carried out to demonstrate the electrochemical signaling mechanism. Finally, this

method has the potential of serving as a basic technology for the development of a portable genetic diagnosis system for a POCT purpose.

Acknowledgements

This work was supported by the NRF of Korea (Mid-career Researcher Program) grant funded by the Korean government (MEST) (No. 2009-0080602 and No. R01-2007-000-11851-0) and the Brain Korea 21 (BK21) Program. Research by S.B.L. was also supported by the WCU program through the KOSEF funded by the MEST (No. R31-2008-000-10071-0).

References

1 J. Wilhelm and A. Pingoud, *ChemBioChem*, 2003, **4**, 1120–1128.
2 H. D. VanGuilder, K. E. Vrana and W. M. Freeman, *BioTechniques*, 2008, **44**, 619–626.
3 M. J. Espy, J. R. Uhl, L. M. Sloan, S. P. Buckwalter, M. F. Jones, E. A. Vetter, J. D. C. Yao, N. L. Wengenack, J. E. Rosenblatt, F. R. Cockerill and T. F. Smith, *Clin. Microbiol. Rev.*, 2006, **19**, 165–256.
4 E. Bakker, *Anal. Chem.*, 2004, **76**, 3285–3298.
5 B. Y. Won, D. W. Lee, S. C. Shin, D. Y. Cho, S. S. Lee, H. C. Yoon and H. G. Park, *Biosens. Bioelectron.*, 2008, **24**, 665–669.
6 B. Y. Won, H. C. Yoon and H. G. Park, *Analyst*, 2008, **133**, 100–104.
7 B. Y. Won, S. C. Shin, W. Chung, S. J. Shin, D. Y. Cho and H. G. Park, *Chem. Commun.*, 2009, 4230–4232.
8 S. S. W. Yeung, T. M. H. Lee and I. M. Hsing, *J. Am. Chem. Soc.*, 2006, **128**, 13374–13375.
9 S. S. W. Yeung, T. M. H. Lee and I. M. Hsing, *Anal. Chem.*, 2008, **80**, 363–368.
10 M. F. Sistare, S. J. Codden, G. Heimlich and H. H. Thorp, *J. Am. Chem. Soc.*, 2000, **122**, 4742–4749.
11 P. M. Armistead and H. H. Thorp, *Bioconjugate Chem.*, 2002, **13**, 172–176.
12 V. A. Szalai and H. H. Thorp, *J. Am. Chem. Soc.*, 2000, **122**, 4524–4525.
13 M. E. Napier, C. R. Loomis, M. F. Sistare, J. Kim, A. E. Eckhardt and H. H. Thorp, *Bioconjugate Chem.*, 1997, **8**, 906–913.
14 I. V. Yang, P. A. Ropp and H. H. Thorp, *Anal. Chem.*, 2002, **74**, 347–354.
15 T. Defever, M. Druet, M. Rochelet-Dequaire, M. Joannes, C. Grossiord, B. Limoges and D. Marchal, *J. Am. Chem. Soc.*, 2009, **131**, 11433–11441.
16 M. T. Carter and A. J. Bard, *J. Am. Chem. Soc.*, 1987, **109**, 7528–7530.
17 M. T. Carter, M. Rodriguez and A. J. Bard, *J. Am. Chem. Soc.*, 1989, **111**, 8901–8911.
18 M. Kobayashi, K. B. Takashi, M. Saito, S. Kaji, M. Oomura, S. Iwabuchi, Y. Morita, Q. Hasan and E. Tamiya, *Electrochem. Commun.*, 2004, **6**, 337–343.
19 A. Erdem, K. Kerman, B. Meric, U. S. Akarca and M. Ozsoz, *Anal. Chim. Acta*, 2000, **422**, 139–149.
20 A. Erdem, K. Kerman, B. Meric and M. Ozsoz, *Electroanalysis*, 2001, **13**, 219–223.
21 P. Kara, K. Kerman, D. Ozkan, B. Meric, A. Erdem, Z. Ozkan and M. Ozsoz, *Electrochem. Commun.*, 2002, **4**, 705–709.
22 E. M. Boon, D. M. Ceres, T. G. Drummond, M. G. Hill and J. K. Barton, *Nat. Biotechnol.*, 2000, **18**, 1096–1100.
23 A. J. Wain and F. M. Zhou, *Langmuir*, 2008, **24**, 5155–5160.
24 M. Hossain, P. Giri and G. S. Kumar, *DNA Cell Biol.*, 2008, **27**, 81–90.
25 M. Hossain and G. S. Kumar, *Mol. BioSyst.*, 2009, **5**, 1311–1322.
26 B. S. Fujimoto, J. B. Clendenning, J. J. Delrow, P. J. Heath and M. Schurr, *J. Phys. Chem.*, 1994, **98**, 6633–6643.
27 S. Nafisi, A. A. Saboury, N. Keramat, J. F. Neault and H. A. Tajmir-Riahi, *J. Mol. Struct.*, 2007, **827**, 35–43.
28 T. H. Fang, N. Ramalingam, X. D. Dong, T. S. Ngin, X. T. Zeng, A. T. L. Kuan, E. Y. P. Huat and H. Q. Gong, *Biosens. Bioelectron.*, 2009, **24**, 2131–2136.
29 M. H. Shapero, K. K. Leuther, A. Nguyen, M. Scott and K. W. Jones, *Genome Res.*, 2001, **11**, 1926–1934.
30 A. Pemov, H. Modi, D. P. Chandler and S. Bavykin, *Nucleic Acids Res.*, 2005, **33**.
31 U. Eskiocak, D. Ozkan-Ariksoysal, M. Ozsoz and H. A. Oktem, *Anal. Chem.*, 2007, **79**, 8807–8811.
32 D. H. Evans, *J. Electroanal. Chem.*, 1989, **258**, 451–456.
33 F. L. Almeida, M. B. A. Fontes, C. Jimenez and I. Burdallo, *ECS Trans.*, 2008, **14**, 73–82.
34 R. P. Baldwin, T. J. Roussel, M. M. Crain, V. Bathlagunda, D. J. Jackson, J. Gullapalli, J. A. Conklin, R. Pai, J. F. Naber, K. M. Walsh and R. S. Keynton, *Anal. Chem.*, 2002, **74**, 3690–3697.
35 O. Bagasra, *Nat. Protoc.*, 2007, **2**, 2782–2795.
36 C. M. Carey and W. B. Riggan, *Anal. Chem.*, 1994, **66**, 3587–3591.
37 D. Xiao, H. Y. Yuan, J. Li and R. Q. Yu, *Anal. Chem.*, 1995, **67**, 288–291.
38 R. K. Meruva and M. E. Meyerhoff, *Anal. Chem.*, 1996, **68**, 2022–2026.
39 Y. Makino, T. Mori and Y. Abe, JP2003047500A, 2003.
40 A. M. O. Brett and S. H. P. Serrano, *J. Brazil. Chem. Soc.*, 1995, **6**, 97–100.
41 P. Singhal and W. G. Kuhr, *Anal. Chem.*, 1997, **69**, 4828–4832.
42 W. R. Yang, M. Ozsoz, D. B. Hibbert and J. J. Gooding, *Electroanalysis*, 2002, **14**, 1299–1302.
43 J. Liu, T. X. Zhang, T. B. Lu, L. H. Qu, H. Zhou, Q. L. Zhang and L. N. Ji, *J. Inorg. Biochem.*, 2002, **91**, 269–276.
44 R. Zana and R. A. Mackay, *Langmuir*, 1986, **2**, 109–113.
45 M. J. Eddowes and M. Gratzel, *J. Electroanal. Chem.*, 1984, **163**, 31–64.
46 T. Matsue, D. H. Evans, T. Osa and N. Kobayashi, *J. Am. Chem. Soc.*, 1985, **107**, 3411–3417.
47 G. N. Kamau, T. Leipert, S. S. Shukla and J. F. Rusling, *J. Electroanal. Chem.*, 1987, **233**, 173–187.
48 J. F. Rusling, C. N. Shi and T. F. Kumosinski, *Anal. Chem.*, 1988, **60**, 1260–1267.